RESEARCH ARTICLE

NANO · MICRO small
www.small-journal.com

Ferromagnetic Boundary States in the Hydrogenated Graphene/Nickel Moiré Superlattice

Yang Song, Shixuan Du, Feng Liu, and Lizhi Zhang**

Zigzag graphene nanoribbons (ZGNRs) exhibit spin-polarized edge states, which are key elements for designing graphene-based spintronics devices. The intrinsic ZGNRs have an antiferromagnetic ground state, which can be modified by edge engineering and external field. Here, this work proposes an avenue to realize the zigzag graphene/graphane nanoribbon superlattice (ZGNR-SL) on Ni(100) by selective hydrogenation of the 1D moiré patterns, based on the first-principles calculations. The growth mechanism of the ZGNR-SL is revealed having two steps: first, hydrogen atoms intercalate at the interface of graphene/Ni and form H ribbons in the apex regions of the 1D moiré pattern; second, the intercalated hydrogen ribbons serve as a template for the directed hydrogen adsorption on both sides of the graphene over the hydrogen ribbons. Interestingly, ZGNR-SL on Ni(100) surface exhibit ferromagnetic boundary states, which may be exploited in potential spintronics device applications.

1. Introduction

Graphene nanoribbons (GNRs) have been extensively investigated because they exhibit many interesting electronic and magnetic properties, which are largely controlled by their edge geometries.[1,2] For example, a zigzag graphene nanoribbon (ZGNR) with perfect straight edges has spin-polarized edge states in an antiferromagnetic (AFM) ground state,[3–8] which can be made ferromagnetic (FM) by modifying edge shapes[9] while edge magnetic moments can be suppressed by edge defects.[10] The AFM ZGNR can be made into half metal,[11] while a FM sawtooth GNR can be made into a spin semiconductor,[12] by applying a transverse electric field across the ribbon. Both FM and AFM magnetic superlattice can be designed by graphene nanoholes with zigzag edges[13] for magnetic memory device. The AFM ZGNR has been proposed to construct giant magnetoresistance devices,[14,15] and spin photogalvanic devices.[16]

Up to now, various methods have been employed to fabricate GNRs, primarily falling into two broad categories: a top-down approach of patterning of graphene sheets,[17–22] and a bottom-up approach of growing graphene nanoribbons from molecular precursors.[8,23–25] The top-down approach, such as e-beam[17] and ion-beam[26] lithography, scanning tunneling microscope lithography,[18] and sonochemical unzipping of graphene nanotubes,[19–22] may produce edge irregularities and unpredictable substitutions of carbon atoms, which affect the conductive properties of GNRs. On the other hand, the bottom-up approach, such as surface-catalyzed cyclodehydrogenation strategies,[23–25] face the challenge of limited ribbon length. Therefore, continued efforts need to be made in developing new strategies to synthesize high-quality and longer GNRs.

Besides fabricating GNRs, two complementary methods have been employed in making one- or two-dimensional (1D or 2D) superlattice structures. One method is by annealing 2D material to fabricate defects and deposit atoms on 2D material by molecular beam epitaxy, where annealing causes linear defects to align regularly with a uniform interval and transforms the homogeneous monolayer VSe_2 phase into 1D-patterned monolayer VSe_2 phase.[27] The other method is by depositing H atoms on moiré pattern of Gr/Ru(0001) system, where honeycomb-patterned hydrogenated graphene (HPHG) is fabricated.[28] Hydrogen functionalization of graphene is used as an effective method to introduce novel electronic and mechanical properties, such as band gap tuning,[29] magnetic properties controlling[30] and structure bending and folding.[31,32] By using density-functional-theory (DFT) calculations, the growth mechanism of HPHG that uses the intercalated H buffer layer as a template to guide the hydrogenation process has been revealed. Inspired by the growth of HPHG, a 2D-patterned material, we aimed to realize 1D-patterned hydrogenated graphene grown on metal substrate and

Y. Song, L. Zhang
Laboratory of Theoretical and Computational Nanoscience
National Center for Nanoscience and Technology
Beijing 100190, China
E-mail: zhanglz@nanoctr.cn
Y. Song, S. Du
Beijing National Laboratory for Condensed Matter Physics and Institute of Physics
Chinese Academy of Sciences
Beijing 100190, China
E-mail: sxdu@iphy.ac.cn
Y. Song, S. Du
University of Chinese Academy of Sciences
Chinese Academy of Sciences
Beijing 100190, China
F. Liu
Department of Materials Science and Engineering
University of Utah
Salt Lake City, Utah 84112, USA

The ORCID identification number(s) for the author(s) of this article can be found under https://doi.org/10.1002/smll.202411646

DOI: 10.1002/smll.202411646

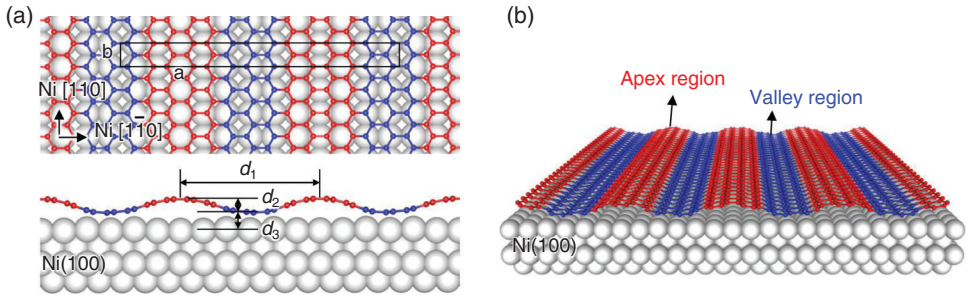

Figure 1. The atomic structures of 1D moiré pattern of graphene on Ni(100) surface. a) The top and side views of graphene adsorbed on Ni(100). 1D moiré pattern arise from the mismatch between graphene and substrate. The carbon atoms in apex and valley regions are marked by red and blue, respectively. The rectangular boxes mark the primitive cells. b) Perspective view for showing the 1D moiré pattern.

synchronously obtained a zigzag graphene/graphane nanoribbon superlattice (ZGNR-SL), which shows similar electronic and magnetic properties with the isolated ZGNRs.[7,11,33,34]

In the present work, we propose to realize ZGNR-SL on a Ni(100) substrate by selective hydrogenation of the 1D moiré patterns, graphene/Ni(100) (Gr/Ni(100)), for which the Gr/Ni(100) with 1D moiré pattern have been already synthesized.[35,36] Based on first-principles calculations, we predict the growth mechanism of ZGNR-SL, which consists of two steps: intercalation and hydrogenation. In the intercalation step, hydrogen atoms intercalate at the interface of Gr/Ni(100) and bond to the substrate in the apex regions of a 1D moiré pattern. As the hydrogen coverage increases, the intercalated hydrogen atoms gradually fill the interface under the apex regions, producing a hydrogen buffer layer in the form of ribbons. In the hydrogenation step, the intercalated hydrogen buffer layer serves as a template to guide hydrogen adsorption preferentially on both sides of the graphene over the hydrogen buffer layer, transforming the sp^2 to sp^3 C-C bonds. Consequently, a superlattice of ZGNRs is formed after graphene in the original apex regions is hydrogenated. Moreover, selective hydrogenation induces spin density rearrangement, and ZGNR-SL on Ni(100) surface exhibits a FM spin-polarized boundary states, in contrast to the AFM ground state of the isolated ZGNRs with perfect straight edges.[7,8] This process provides an alternative approach for graphene nanoribbon-based applications.

2. Results and Discussion

The Gr/Ni(100) with 1D moiré pattern along the zigzag edge of graphene has been synthesized in experiments.[35,36] We replicated the structure used as the experimental and DFT models in the reference.[35] Due to lattice mismatch and periodic interaction strengths, the monolayer graphene on Ni(100) features a 1D moiré pattern. The top and side views of Gr/Ni(100) are shown in **Figure 1**a. The width of the 1D moiré pattern in Gr/Ni(100) model, d_1, is 14.72 Å. The height of the ripple in Gr/Ni(100) (d_2) is 1.43 Å, and the distance between the lowest position of graphene and the first atomic layer of Ni(100) substrate, d_3, is 1.90 Å, which indicates strong interaction between graphene and Ni substrate. To show the moiré pattern along zigzag direction clearly, the carbon atoms in apex regions (higher regions) and valley regions (lower regions) of 1D ripple are marked by red and blue, respectively. Gr/Ni(100) is simulated by using a $(7\sqrt{3} \times 1)$ graphene sitting on a (12×1) Ni(100) model, whose lattice constants are: a = 29.44 Å, b = 2.45 Å, which is consistent with the reported experiment results.[35,36] Additionally, we also tried to find other possible structures and confirmed that the Gr/Ni(100) model is the ground state (see details in Figure S1, Supporting Information). Furthermore, the perspective view in Figure 1b shows the 1D ripple three-dimensionally.

The intercalation of H atoms is very common for many Gr/metal systems.[28,37,38] To confirm the most preferable adsorption site for H atoms in the Gr/Ni(100) system, we first considered a few of H atoms interact with Gr/Ni(100) system. **Figure 2**a–c show the most energy favorable configurations considering adsorption of 1, 4, and 8 H atoms, respectively. We considered several possible configurations for each H coverage as shown in Figures S2 and S3, Supporting Information. No matter how many H atoms we considered, the adsorption of H atoms in the valley region has a higher binding energy, indicating energy instability. The final state in the intercalation process is shown in Figure 2c, in which H atoms on Ni(100) form a line-patterned intercalated H layer. In the side view, the ripple is maintained during the intercalation process. To figure out the diffusion behavior of intercalated H atoms on the 1D moiré pattern, we calculate the diffusion barriers for H adsorbed in the center of the apex region to the valley region (Figure 2d). First, we find that the H diffusion barrier globally increases from the apex region to the valley region (Figure 2e), suggesting that intercalated H atoms can easily diffuse in the apex regions, but hardly diffuse in the valley regions. Second, the relative total energy increases along the diffusion pathway, indicating that H atoms would only fill up the apex regions if limited H atoms are provided. What's more, there is a couple of asymmetric barriers on the boundary between apex region and valley region. The energy barrier is 0.35 eV from site 3 to site 5, while it is only 0.07 eV in the opposite direction, indicating that even if a H atom can overcome the 0.35 eV barrier to the valley region, it can easily diffuse back, which means H atoms adsorb in apex regions.

After the intercalation process, a line-patterned H layer is intercalated into the Gr/Ni(100) interface in the apex regions (**Figures** 2c and 3a). Based on this configuration, we will explore the hydrogenation process of the rippled graphene. We propose double-sided hydrogenated configurations in apex regions and up-sided hydrogenated configurations in valley regions with low (Figure S4a,b, Supporting Information) and high (Figure S4c,d, Supporting Information) H coverages, where the binding energy

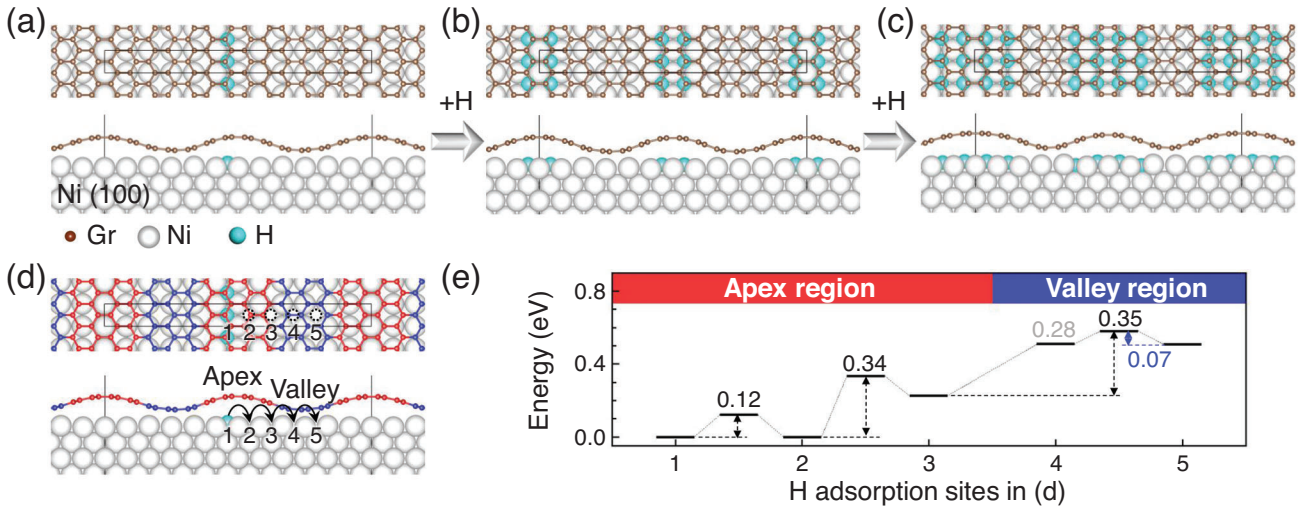

Figure 2. Intercalation process of H atoms at the Gr/Ni(100) interface. a–c) The top and side view of the atomic structure for each step in the intercalation process: (a) one H atom, (b) four H atoms and (c) eight H atoms per unit cell intercalate under apex regions. d) The diffusion path for an intercalated H atom diffusing from an apex to a valley region. The small dotted circles with corresponding numbers mark the adsorption sites on Ni(100) surface. e) The diffusion barriers for a H atom diffusing along the path in (d).

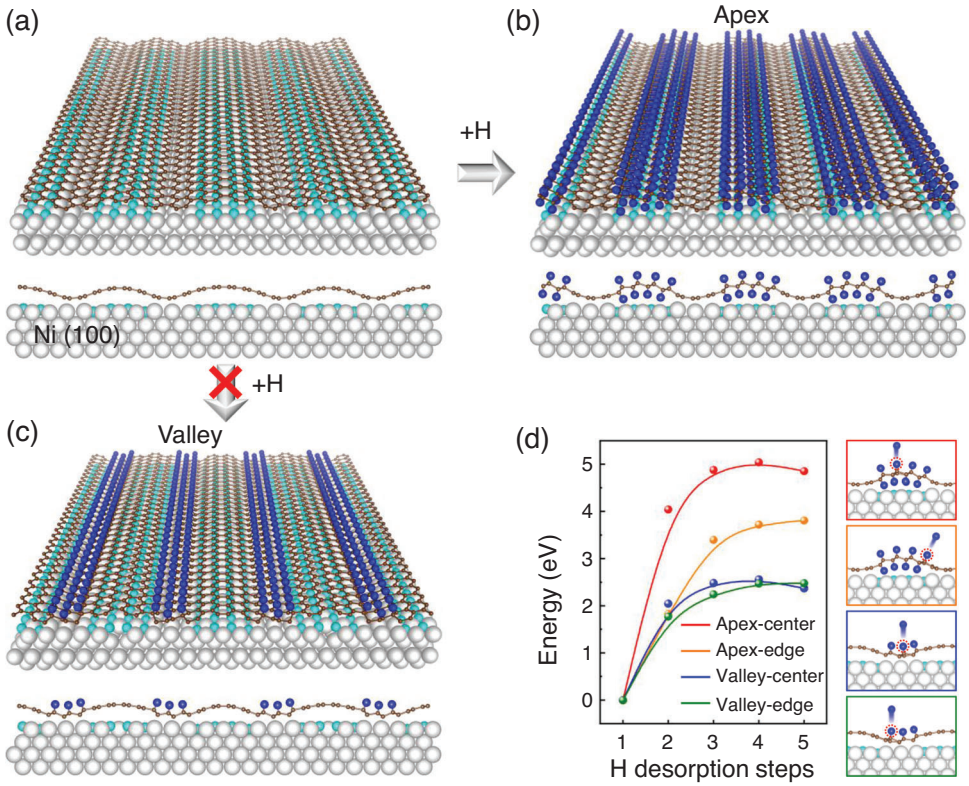

Figure 3. Growth mechanism of ZGNR-SL on Ni(100). a) Perspective view and side view of Gr/Ni(100) with line-patterned intercalated H layer. b) H atoms adsorb on both sides of graphene in the apex regions. c) H atoms adsorb on the upper side of graphene in the valley regions. d) Energy barriers of H desorption from the upper side of graphene in ZGNR-SL/Ni(100) in (b) (the red/orange lines) and (c) (the blue/green lines). The insets on the right side show the schematic of H desorption process.

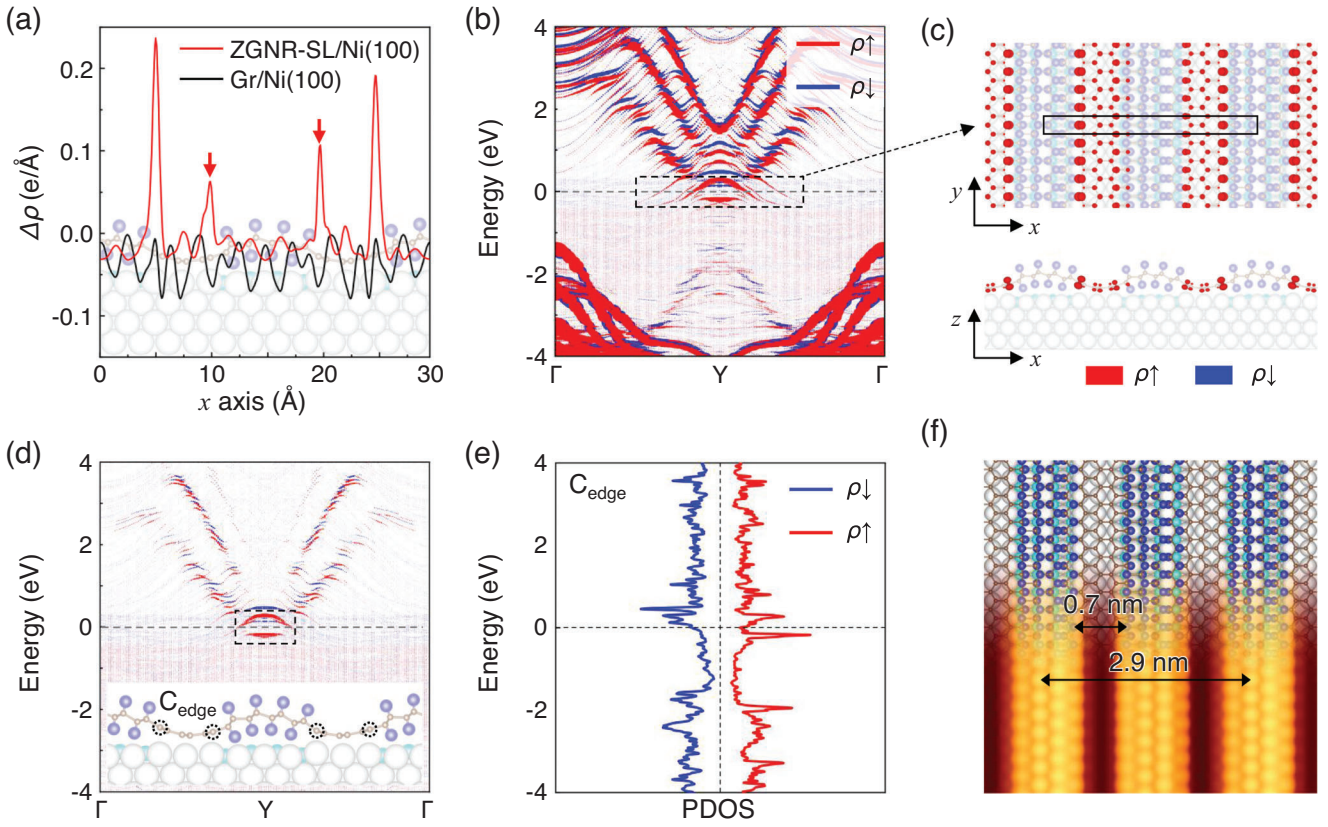

Figure 4. Electronic and magnetic properties of ZGNR-SL on Ni(100) substrate. a) Spin charge density difference ($\Delta\rho$, $\rho\uparrow - \rho\downarrow$) distribution along x axis of Gr/Ni(100) before (black line) and after (red line) hydrogenation. The integral region only includes Gr (or HGr) layer. b) Projected band structure of the carbon skeleton of ZGNR-SL on Ni(100) substrate, where the spin-up and spin-down bands are marked by red and blue. The weights of electronic states are marked by the size of dots. c) Top and side views of ZGNR-SL/Ni(100) show the distribution of the spin charge density differences ($\rho\uparrow - \rho\downarrow$) in the energy range of (−0.3 eV, 0.3 eV). The isosurfaces of $\Delta\rho\uparrow$ and $\Delta\rho\downarrow$ charge density are marked by red and blue, respectively. The isosurface is chosen as 0.004 e bohr^{-3}. The charge density of Ni substrate is not shown in order to provide a clear view of the magnetic structure of the ZGNR-SL. d) Projected band structure of the C atoms on the boundary. e) Spin-dependent PDOS projected on C atoms on the boundary marked in (d). f) Atomic configuration and related STM simulation for ZGNR-SL on Ni(100). The energy range is from −1 eV to the fermi level.

per H atom is calculated by the formula: $E_b = (E_{nH/Gr/8H/Ni} - E_{Gr/8H/Ni} - n \times E_H)/n$. We find that E_b of double-sided hydrogenation in the apex regions is lower than that of single-sided hydrogenation in the valley regions by 0.17/0.65 eV per H atom at low/high H coverage, indicating that H atoms prefer to adsorb on opposite sides of graphene in the apex regions. To confirm that the valley regions remain as pristine graphene, we performed additional calculations. First, we carried out NEB calculations for H diffusion on the upper side of graphene (Figure S5, Supporting Information). A significant energy barrier of 1.83 eV hinders H diffusion from the apex to the valley regions. Notably, the total energy of the end state is 1.10 eV higher than that of the initial state, which is consistent with the energy relationships in Figure S4, Supporting Information and suggests that H atoms favor the apex regions, although they may occasionally reach the valleys. In addition, Figure 3d illustrates the H desorption energy barriers for ZGNR-SL/Ni(100): 4.9/3.8 eV (red/orange line) at the apex center/edge and 2.6/2.5 eV (blue/green line) at the valley center/edge. The lower barriers imply that H atoms in valley regions are likely to desorb during the annealing process in experiments. In contrast, H atoms located in the apex regions, particularly at the center, exhibit higher stability and are hard to desorb.[28]

In the following, we focus on the electronic and magnetic properties of the ZGNR-SL on Ni(100). **Figure** 4a shows the spin charge density difference ($\Delta\rho$, $\rho\uparrow - \rho\downarrow$) distribution along x axis of Gr/Ni(100) before (black line) and after (red line) hydrogenation. The tiny spin-polarized edge states in the unhydrogenated Gr/Ni(100) system indicates that spin polarization in ZGNR-SL/Ni(100) mainly arises from the hydrogenation. The nickel substrate suppresses the edge states when the edge C atoms go closer to the Ni substrate (see the two peaks in Figure 4a marked by red arrows). The four prominent positive peaks in the red curve indicate a FM state, which suggests that hydrogenation leads to a rearrangement of spin density and thereby enhances ferromagnetism. The spin-polarized projected band structure of the carbon skeleton of ZGNR-SL/Ni(100) in Figure 4b also denotes a FM state. The structure and the FM edge states of ZGNR-SL on Ni(100) is robust even there are a few intercalated H atoms (Figure S6a–c, Supporting Information). Comparing ZGNR-SL/Ni(100) with and without intercalated H atoms (Figure S6a–c,d, Supporting Information), we find

that the intercalated H atoms assist in maintaining the FM edge states of ZGNR-SL. The spatial distribution of $\Delta\rho$ in the energy range of (−0.3 eV, 0.3 eV) (Figure 4c) represents the typical characteristics of ZGNR in a FM state as the boundary states on the two opposite edges possess the same polarized direction. It has been demonstrated that the isolated GNRs with the zigzag edge that are narrower than 7 nanometers are AFM and exhibit an electronic bandgap of about 0.2 – 0.3 eV.[7] The spin-polarized calculations show that the ground state of freestanding ZGNR-SL is also AFM with a bandgap of 0.56 eV (Figure S7, Supporting Information). In other word, ZGNR-SL transforms from an AFM state to a FM state on Ni(100) surface. We also provide the projected band structure and PDOS of the C atoms (shown in the inset of Figure 4d) on the boundary of the ZGNR-SL in Figure 4d,e, which proves that the boundary states localized at the Fermi level. It has been reported that H-terminated ZGNRs on Au(111)[6] and Sb_2Te_3 (an isolator)[39] substrates retain AFM states, which is due to the weak interaction and negligible charge transfer between the ZGNRs and the substrates. While the H-terminated ZGNRs on Ag/Cu(111) exhibit FM edge states, which originate from the relatively stronger interaction between the ZGNR and the substrate.[6] Here, the FM state in ZGNR-SL is probably due to both the magnetic interaction and the charge transfer between ZGNR-SL and the FM Ni(100) substrate.

Therefore, 1D ferromagnetic superlattices are presented in theory and are highly expected to possess promising applications in spintronics. STM simulations are calculated to provide more visual information for future experiments. In Figure 4f, the simulated STM image merged with the atomic structures shows a clear 1D moiré pattern, whose period is 1.45 nm (half of the length of the supercell, 2.9 nm). The widths of the GNRs in ZGNR-SL is 0.5 nm. Furthermore, based on the two-step growth mechanism, ZGNR-SL or other GNR-SLs with other nanoribbon widths can be obtained on other metal substrates, such as Gr/Ni(110)[40,41] and Gr/Cu(110).[42] The exfoliation energy calculations in Table S1 indicate that the ZGNR-SL can be easily split from Ni substrates. We have performed calculations to identify the thermodynamic stability for the freestanding ZGNR-SL (Figure S8, Supporting Information). The ab initio molecular dynamics simulation at 300 K show minor fluctuations in the free energy and a stable atomic structure, confirming the good thermodynamic stability of ZGNR-SL.

3. Conclusion

In summary, we construct a zigzag graphene/graphane nanoribbon superlattice on Ni(100) substrate by partial hydrogenation of the 1D moiré pattern theoretically. Hydrogenation induces the arrangement of spin density distribution and enhances the magnetism. The boundary states of ZGNR-SL on Ni surface exhibit FM distribution, while the freestanding ZGNR-SL exhibit similar electronic and magnetic properties with the isolated ZGNRs. The exfoliation energy calculations indicate that ZGNR-SL can be easily split from Ni substrate. This new strategy is expected to synthesize large-scale and high-quality ZGNR-SLs, which possess potential applications in graphene-based spintronics.

4. Experimental Section

Density-functional-theory calculations were performed using projector-augmented wave (PAW)[43,44] pseudopotentials combining with the Perdew–Burke–Ernzerhof (PBE) exchange-correlation functional,[45,46] as implemented in the Vienna Ab-initio Simulation Package (VASP).[47,48] The energy cutoff of plane-wave basis was set to 500 eV. All the hydrogenated graphene on Ni(100) systems were modelled by ($7\sqrt{3} \times 1$) graphene supercells on a four layered (12×1) supercell of Ni(100) slab. For both models, the lower two layers were fixed, the upper two layers and hydrogenated graphene were totally relaxed until the force on each of the relaxed atoms was smaller than 0.02 eV $Å^{-1}$. The thicknesses of vacuum layers were all larger than 15 Å. The Brillouin zone for hydrogenated graphene on Ni(100) system was sampled by a ($1 \times 12 \times 1$) Γ-centered **k**-mesh.[49] The Grimme-D3 method[50] was used to describe the van der Waals interaction between graphene and Ni substrate.

We calculated the diffusion barrier of a single H atom diffusing on Ni(100) substrate and graphene and the desorption barrier of a single H atom desorbing from hydrogenated graphene. These diffusion and desorption processes were simulated using the climbing image nudged elastic band (CI-NEB) method.[51,52] All the systems in NEB calculations were modelled by ($1 \times 4 \times 1$) supercells. Before the CI-NEB calculations, the initial and final structures were relaxed until the residual force on each of the relaxed atoms was smaller than 0.05 eV $Å^{-1}$. In the CI-NEB calculations, three intermediate states were constructed by using linear interpolation, and the limit of force convergence was set to 0.05 eV $Å^{-1}$. In addition, structures in Figures 4a and S6, Supporting Information were modelled by ($1 \times 5 \times 1$) supercells.

Supporting Information

Supporting Information is available from the Wiley Online Library or from the author.

Acknowledgements

The research was carried out at the National Supercomputer Center in Tianjin, and the calculations were performed on TianHe-1(A). This work was supported in part by the Key R&D of the Ministry of Science and Technology (No. 2022YFA1204103) and the National Natural Science Foundation of China (No. 22372047, No. 12404201).

Conflict of Interest

The authors declare no conflict of interest.

Data Availability Statement

The data that support the findings of this study are available from the corresponding author upon reasonable request.

Keywords

ferromagnet, graphene, hydrogenation, nanoribbon, superlattice

Received: December 3, 2024
Published online:

[1] L. Brey, H. A. Fertig, *Phys. Rev. B* **2006**, *73*, 235411.
[2] O. V. Yazyev, R. B. Capaz, S. G. Louie, *Phys. Rev. B* **2011**, *84*, 115406.

[3] K. Nakada, M. Fujita, G. Dresselhaus, M. S. Dresselhaus, *Phys. Rev. B* **1996**, *54*, 17954.
[4] M. Wimmer, İ. Adagideli, S. Berber, D. Tománek, K. Richter, *Phys. Rev. Lett.* **2008**, *100*, 177207.
[5] O. V. Yazyev, M. I. Katsnelson, *Phys. Rev. Lett.* **2008**, *100*, 047209.
[6] Y. Li, W. Zhang, M. Morgenstern, R. Mazzarello, *Phys. Rev. Lett.* **2013**, *110*, 216804.
[7] G. Z. Magda, X. Jin, I. Hagymási, P. Vancsó, Z. Osváth, P. Nemes-Incze, C. Hwang, L. P. Biró, L. Tapasztó, *Nature* **2014**, *514*, 608.
[8] P. Ruffieux, S. Wang, B. Yang, C. Sánchez-Sánchez, J. Liu, T. Dienel, L. Talirz, P. Shinde, C. A. Pignedoli, D. Passerone, T. Dumslaff, X. Feng, K. Müllen, R. Fasel, *Nature* **2016**, *531*, 489.
[9] D. Yu, E. M. Lupton, H. J. Gao, C. Zhang, F. Liu, *Nano Res.* **2008**, *1*, 497.
[10] B. Huang, F. Liu, J. Wu, B.-L. Gu, W. Duan, *Phys. Rev. B* **2008**, *77*, 153411.
[11] Y.-W. Son, M. L. Cohen, S. G. Louie, *Nature* **2006**, *444*, 347.
[12] Z. F. Wang, S. Jin, F. Liu, *Phys. Rev. Lett.* **2013**, *111*, 096803.
[13] D. Yu, E. M. Lupton, M. Liu, W. Liu, F. Liu, *Nano Res.* **2008**, *1*, 56.
[14] F. Muñoz-Rojas, J. Fernández-Rossier, J. J. Palacios, *Phys. Rev. Lett.* **2009**, *102*, 136810.
[15] Z. F. Wang, F. Liu, *Appl. Phys. Lett.* **2011**, *99*, 042110.
[16] P. Jiang, X. Tao, H. Hao, Y. Liu, X. Zheng, Z. Zeng, *npj Quantum Inf.* **2021**, *7*, 21.
[17] M. Y. Han, B. Özyilmaz, Y. Zhang, P. Kim, *Phys. Rev. Lett.* **2007**, *98*, 206805.
[18] L. Tapasztó, G. Dobrik, P. Lambin, L. P. Biró, *Nat. Nanotechnol.* **2008**, *3*, 397.
[19] X. Li, X. Wang, L. Zhang, S. Lee, H. Dai, *Science* **2008**, *319*, 1229.
[20] D. V. Kosynkin, A. L. Higginbotham, A. Sinitskii, J. R. Lomeda, A. Dimiev, B. K. Price, J. M. Tour, *Nature* **2009**, *458*, 872.
[21] L. Jiao, L. Zhang, X. Wang, G. Diankov, H. Dai, *Nature* **2009**, *458*, 877.
[22] L. Xie, H. Wang, C. Jin, X. Wang, L. Jiao, K. Suenaga, H. Dai, *J. Am. Chem. Soc.* **2011**, *133*, 10394.
[23] J. Cai, P. Ruffieux, R. Jaafar, M. Bieri, T. Braun, S. Blankenburg, M. Muoth, A. P. Seitsonen, M. Saleh, X. Feng, K. Müllen, R. Fasel, *Nature* **2010**, *466*, 470.
[24] S. Linden, D. Zhong, A. Timmer, N. Aghdassi, J. H. Franke, H. Zhang, X. Feng, K. Müllen, H. Fuchs, L. Chi, H. Zacharias, *Phys. Rev. Lett.* **2012**, *108*, 216801.
[25] P. P. Shinde, J. Liu, T. Dienel, O. Gröning, T. Dumslaff, M. Mühlinghaus, A. Narita, K. Müllen, C. A. Pignedoli, R. Fasel, P. Ruffieux, D. Passerone, *Carbon* **2021**, *175*, 50.
[26] Y. Zhang, C. Hui, R. Sun, K. Li, K. He, X. Ma, F. Liu, *Nanotechnology* **2014**, *25*, 135301.
[27] Z.-L. Liu, B. Lei, Z.-L. Zhu, L. Tao, J. Qi, D.-L. Bao, X. Wu, L. Huang, Y.-Y. Zhang, X. Lin, Y.-L. Wang, S. Du, S. T. Pantelides, H.-J. Gao, *Nano Lett.* **2019**, *19*, 4897.
[28] Y. Song, K. Qian, L. Tao, Z. Wang, H. Guo, H. Chen, S. Zhang, Y.-Y. Zhang, X. Lin, S. T. Pantelides, S. Du, H.-J. Gao, *Small* **2022**, *18*, 2102687.
[29] D. Haberer, D. V. Vyalikh, S. Taioli, B. Dora, M. Farjam, J. Fink, D. Marchenko, T. Pichler, K. Ziegler, S. Simonucci, M. S. Dresselhaus, M. Knupfer, B. Buchner, A. Gruneis, *Nano Lett.* **2010**, *10*, 3360.
[30] Y. Song, L. Tao, Y. Zhang, J. Pan, S. Du, *Chem. Res. Chin. Univ.* **2021**, *37*, 1110.
[31] D. Yu, F. Liu, *Nano Lett.* **2007**, *7*, 3046.
[32] Z. F. Wang, Y. Zhang, F. Liu, *Phys. Rev. B* **2011**, *83*, 041403.
[33] J.-H. Lee, J. C. Grossman, *Phys. Rev. B* **2011**, *84*, 113413.
[34] J.-H. Lee, J. C. Grossman, *Appl. Phys. Lett.* **2010**, *97*, 133102.
[35] Z. Zou, V. Carnevali, M. Jugovac, L. L. Patera, A. Sala, M. Panighel, C. Cepek, G. Soldano, M. M. Mariscal, M. Peressi, G. Comelli, C. Africh, *Carbon* **2018**, *130*, 441.
[36] A. Sala, Z. Zou, V. Carnevali, M. Panighel, F. Genuzio, T. O. Menteş, A. Locatelli, C. Cepek, M. Peressi, G. Comelli, C. Africh, *Adv. Funct. Mater.* **2022**, *32*, 2105844.
[37] H. Chen, D.-L. Bao, D. Wang, Y. Que, W. Xiao, G. Qian, H. Guo, J. Sun, Y.-Y. Zhang, S. Du, S. T. Pantelides, H.-J. Gao, *Adv. Mater.* **2018**, *30*, 1801838.
[38] D. Lizzit, M. I. Trioni, L. Bignardi, P. Lacovig, S. Lizzit, R. Martinazzo, R. Larciprete, *ACS Nano* **2019**, *13*, 1828.
[39] W. Zhang, F. Hajiheidari, Y. Li, R. Mazzarello, *Sci. Rep.* **2016**, *6*, 29009.
[40] D. Usachov, A. M. Dobrotvorskii, A. Varykhalov, O. Rader, W. Gudat, A. M. Shikin, V. K. Adamchuk, *Phys. Rev. B* **2008**, *78*, 085403.
[41] Y. Murata, V. Petrova, B. B. Kappes, A. Ebnonnasir, I. Petrov, Y.-H. Xie, C. V. Ciobanu, S. Kodambaka, *ACS Nano* **2010**, *4*, 6509.
[42] O. Dugerjav, G. Duvjir, L. Tapaszto, C. Hwang, *J. Phys. Chem. C* **2020**, *124*, 12106.
[43] P. E. Blöchl, *Phys. Rev. B* **1994**, *50*, 17953.
[44] G. Kresse, D. Joubert, *Phys. Rev. B* **1999**, *59*, 1758.
[45] J. P. Perdew, K. Burke, M. Ernzerhof, *Phys. Rev. Lett.* **1996**, *77*, 3865.
[46] J. P. Perdew, K. Burke, M. Ernzerhof, *Phys. Rev. Lett.* **1997**, *78*, 1396.
[47] D. Vanderbilt, *Phys. Rev. B* **1990**, *41*, 7892.
[48] G. Kresse, J. Furthmüller, *Phys. Rev. B* **1996**, *54*, 11169.
[49] H. J. Monkhorst, J. D. Pack, *Phys. Rev. B* **1976**, *13*, 5188.
[50] S. Grimme, J. Antony, S. Ehrlich, H. Krieg, *J. Chem. Phys.* **2010**, *132*, 154104.
[51] G. Henkelman, B. P. Uberuaga, H. Jónsson, *J. Chem. Phys.* **2000**, *113*, 9901.
[52] G. Henkelman, H. Jónsson, *J. Chem. Phys.* **2000**, *113*, 9978.